

# Light Intensity Characterization of Plastic Optical Fiber as Gasoline and Diesel Vapor Sensor

Bakti Dwi Waluyo<sup>1</sup>, Mega Silfia Dewy<sup>2</sup>

{bakti\_dw@unimed.ac.id<sup>1</sup>, megasilfiadewy@unimed.ac.id<sup>2</sup>}

Department of Electrical Engineering Education, Faculty of Engineering, Universitas Negeri Medan,  
Medan, Indonesia

**Abstract.** This research produces plastic fiber optic sensors to detect gasoline and diesel vapors. The sensor consists of a single-mode optical fiber which has removed the original 3 cm long cladding in the center and replaced with Stannic Oxide (SnO<sub>2</sub>). The modified cladding coated with SnO<sub>2</sub> can produce attenuation changes at the core and cladding boundaries (evanescent field). This attenuation change is in line with changes in light intensity when interacting with gasoline and diesel vapors. The optical fiber sensor can respond to the concentration of gasoline vapors, with the most optimal sensor sensitivity value being 0.0821 volts/°C at 50 ppm. At the same time, the response to diesel vapors has a sensitivity value of -0.0262 volts/°C at a concentration of 50 ppm. There is a difference in the response of the fiber optic sensor when interacting with gasoline and diesel vapors. When interacting with gasoline vapors, the higher the vapor concentration, the less light intensity received by the OTDR. The higher the concentration of diesel vapor given, the more light intensity received by the OTDR.

**Keywords:** Optical fiber sensor, gasoline vapor, diesel vapor, SnO<sub>2</sub>.

## 1 Introduction

In general, motorized vehicles use gasoline or diesel as fuel. The use of fuel depends on the type of engine used. Gasoline and diesel are obtained from the crude oil refining process. Gasoline can be categorized as a volatile organic compound (VOC) because most gasoline components have a high enough vapor pressure under atmospheric conditions to evaporate easily [1]. Diesel oil is a type of distillate fuel with a clear brownish-yellow color. Diesel oil is obtained in a distillation column at a temperature of 200 °C - 350 °C. Diesel fuel contains 75% saturated hydrocarbons (paraffin, n-paraffin, isoparaffin, and cycloparaffin). The remaining 25% consists of aromatic hydrocarbons (naphthalene and alkylbenzene).

Gasoline and diesel fuel are volatile, so they can cause economic losses and harm the environment around the filling station, especially the people in those locations [2]. In addition to air pollution, the evaporation of gasoline and diesel can also cause human health problems, especially respiratory tract irritation. This condition is exacerbated because gasoline and diesel

vapor have a greater density than air and the residence time in the air is quite long. As a result, gasoline and diesel vapor stays near the filling station for a long time.

So far, many sensors have been developed that are sensitive to detecting vapors from chemicals. Among them is the use of chemical resistors [3], piezo resonance elements [4], and capacitive transducers [5], which have been reported to be able to be used as quality evaluators of gasoline and diesel. This type of sensor uses electrical signals in its operation. Because gasoline and diesel fuel are highly combustible and explosive, using electricity might result in fires. The fact that fiber optic sensors operate without the usage of electrical impulses makes them an appealing substitute. The fiber optic sensor also enables the implementation of highly sensitive measurements and is impervious to electromagnetic interference. [6].

Various kinds of research that have been done on optical fiber to detect gases are the main basis for my research. Research by [7] examined the use of fiber optic sensors to detect gasoline quality. The optical fiber sensor is specifically used to detect pure gasoline or gasoline mixed with other chemicals or substances. The optical fiber sensor is based on a tilted Bragg fiber grating so that the sensor can detect variations in the ethanol concentration in the gasoline-ethanol solution.

Based on research on fiber optic sensors based on ZnO nanoparticles to detect fuel adulteration [8]. The sensor exhibits high sensitivity with various fuel mixtures, ranging from E0 to E100. The sensor is tested for 60 seconds at room temperature to identify the type of mixture fed to the gasoline. The highest sensitivity based on the observations was using a mixture of types E0 followed by E100.

Optical fiber is also used as a sensor to evaluate the mixture of biodiesel and diesel [9]. All the biodiesel and diesel samples used in this study were diluted in cyclohexane in ratios of 1:1 and 1:2. Lower amounts of biodiesel could be detected when the sample BX was diluted in cyclohexane at a ratio of 1:1, which resulted in the fiber optic sensor's sensitivity being at its highest. The volumetric concentration of biodiesel in the mixture, denoted by the letter X, gives the blend of biodiesel and diesel the BX.

This research has produced a prototype device capable of detecting gasoline and diesel vapors. A long-period grating (LPG)-based fiber optic sensor was developed in research [10][11] to detect gasoline mixes, which served as inspiration for this study. Fiber optic sensors based on LPG can also measure the amount of mixed ethanol and other impurities in gasoline [12]. Rodriguez's further work led to the creation a multimode fiber-optic sensor with a sensitivity of 0.270 nm/% for ethanol that can assess the quality of gasoline-ethanol mixtures [13]. Previous studies still have shortcomings, including the need for complex equipment, high costs, and relatively long response times.

An optical time-domain reflectometer (OTDR) is the main device utilized in this investigation to transmit and receive light. The OTDR was selected because it can precisely assess optical fiber in the time domain. Plastic single-mode optical fiber is the type utilized as the sensor. With a diameter of 245  $\mu\text{m}$ , this plastic optical fiber includes a fluorinated polymer exterior protective structure. This outer shield has a refractive index of 1.492 and is usually called cladding. The core structure of the plastic optical fiber is made of polymethyl methacrylate (PMMA). The core is usually called the core, where the core has a diameter of 3.6  $\mu\text{m}$  and a refractive index of 1.464.

Plastic optical fiber can be used as a sensor if the original cladding is replaced with a material sensitive to gasoline or diesel vapor. One material sensitive to gasoline and diesel vapor is Stannic Oxide ( $\text{SnO}_2$ ).  $\text{SnO}_2$  is a nanoparticle found to detect gasoline and diesel vapors.  $\text{SnO}_2$  is used as a cladding on plastic optical fiber using a dip coating technique to make a sensor sensitive to gasoline and diesel vapor.

## 2 Literature Review

### 2.1 Optical Fiber

Optical fiber consists of two important components: the core and the reflection layer (cladding). The principle of transmitting light inside an optical fiber is known as total internal reflection. Total internal reflection in the optical fiber core can be achieved if the refractive index of the core ( $n_1$ ) is greater than the refractive index of the cladding ( $n_2$ ), namely  $n_1 > n_2$  [14], [15]. Figure 1 illustrates the crucial fiber parameters, including (a) critical angle ( $\phi_c$ ), where the ratio of the refractive indices of the cladding and the core determines the value of  $\phi_c$ .

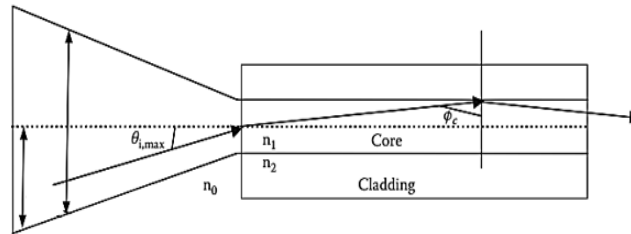


**Fig. 1.** A representation of optical fiber light directing.

Like Equation 1 below:

$$\sin \phi_c = \frac{n_2}{n_1} \quad (1)$$

(b) The acceptance cone angle,  $\theta_{i,max}$ , which depends on the refractive indices of the core, the clad, and the ambient refractive index,  $n_0$ ,

$$\sin \theta_{i,max} = \frac{\sqrt{(n_1^2 - n_2^2)}}{n_0} \quad (2)$$

And (c) the numerical aperture (NA), which defines the fiber's light collection efficiency and is related to the acceptance cone's angle as:

$$NA = n_0 \sin \theta_{i,max} \quad (3)$$

All these parameters are critically important when designing fiber chemical sensors.

### 2.2 Evanescent Wave

Total internal reflection occurs when the incident light is reflected from an interface at an angle larger than the critical angle. However, a small amount of light passes through the reflecting material, and its intensity does not abruptly decrease to zero at the interface. The evanescent wave is the name given to this pierced electromagnetic field, as seen in Figure 2 [16]. The distance required for the electric field amplitude to drop to  $1/e$  (0.37) of its value at

the interface is known as the penetration depth ( $d_p$ ), which depends on the wavelength of the light and the angle of incidence. This is because the amplitude of evanescent waves decays exponentially with distance, as mathematically given by:

$$d_p = \frac{\lambda}{4\pi[n_1^2 \sin^2 \theta - n_2^2]^{1/2}} \quad (4)$$

The transmitted light's wavelength is  $\lambda$ , and the corresponding refractive indices (RI) of the core and cladding are  $n_1$  and  $n_2$ , respectively.

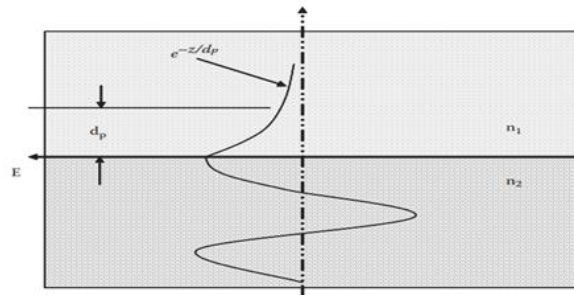


Fig. 2. An illustration of exponential decay of evanescent field.

### 2.3 The Pattern of Synthesize SnO<sub>2</sub>

Figure 3 displays the SnO<sub>2</sub> nanopowders' X-ray diffraction pattern. The generated SnO<sub>2</sub> nanopowders' XRD pattern might be used to identify a rutile tetragonal structure (PCPDF card no-88-0287). The sharp and narrow diffraction peaks corresponding to the unique planes (110), (101), (111), and (211) provide evidence that rutile structured nanopowder was produced [17]. Within the limits of XRD detection, no impurity phases have been found.

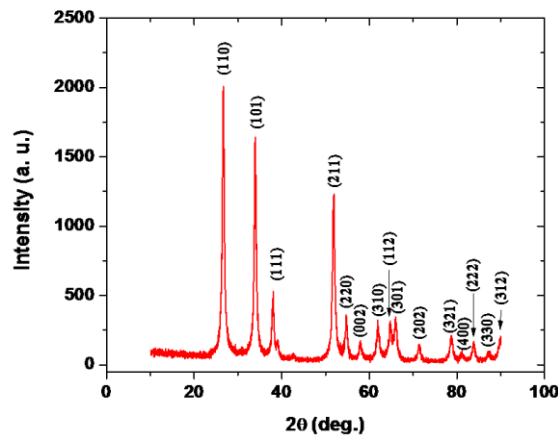


Fig. 3. Synthesized SnO<sub>2</sub> nanopowders' XRD pattern.

Williamson and Hall's (W-H) equation for Cauchy-Lorentzian crystals estimates the average crystallite size of the nanopowders to be 29 nm as given by: [18]

$$\beta \cos \theta = \frac{c \lambda}{D} + 4 \varepsilon \sin \theta \quad (5)$$

Where D is the crystallite size, C is the form factor, which is typically assumed to be 0.89,  $\beta$  is the full width at half maximum (FWHM),  $\theta$  is the Bragg diffraction angle, and  $\lambda$  is the radiation wavelength ( $\lambda=1.54$ ).

### 3 Methods

#### 3.1 Plastic Optical Fiber

I used a single-mode plastic fiber optic with the code 980HP from Thorlabs Inc in this study. The length of the plastic optical fiber used in the study was 60 cm. ST connectors are installed at both ends of the optical fiber. Next, the original 3 cm long cladding layer is removed right in the middle of the plastic optical fiber. The initial cladding was eliminated via a chemical etching process, namely by distributing acetone on the surface of the core. The cladding will thicken due to the chemical etching process and slowly separate from the core. Alcohol is used to clean the original cladding after it has been peeled off. Figure 4 depicts an optical fiber during chemical etching.



Fig. 4. Chemical etching of an optical fiber.

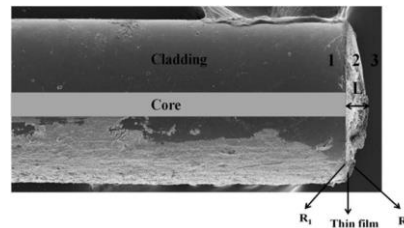


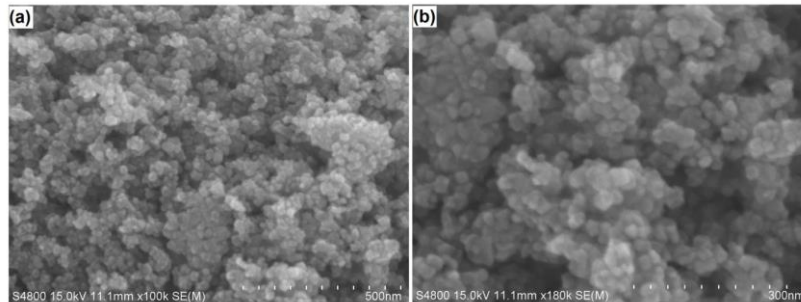
Fig. 5. The plastic optical fiber area is used as the sensor.

Figure 5 depicts the sensor's plastic optical fiber. The fiber-thin film and thin film-air interfaces are included in the fiber tip-coated assembly. The power reflection coefficients of these two reflection surfaces, 1 and 2, are denoted as  $R_1$  and  $R_2$ , respectively. The hollow is thus generated and is L in length.

#### 3.2 SnO<sub>2</sub> Coating

Figures 6a and 6b display the SnO<sub>2</sub> nanopowders' surface morphology at various magnifications. It demonstrates the creation of uniformly dispersed, spherical-shaped nanoparticles with an average size of 275 nm. Most of the nano sol's synthesis involved

hydrolysis and condensation processes. TEOS was specifically hydrolyzed and condensed with deionized water to create the sol that contained nano-silica particles. Conditions such as environmental temperature, catalysts, and solvents also impact the nano sol's characteristics. Figure 7 illustrates how the nano sol films were created depending on experimental settings that were examined using a scanning electron microscope (SEM). The findings showed that the silica particles' average size was 200 nm.



**Fig. 6.** Two different enlargements of SEM images of SnO<sub>2</sub> nanopowders (a) 500 nm and (b) 300 nm.

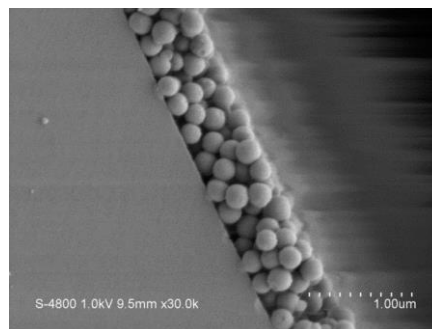


**Fig. 7.** An SEM image of the sensing thin film's nanoparticles on the surface of the optical fiber.

The dip-coating method is used to coat the plastic optical fiber's core. The dip-coating technique is to insert the core of the plastic optical fiber removed from the original cladding into SnO<sub>2</sub>. The steps of the dip-coating technique are that the first SnO<sub>2</sub> is dissolved in water at a temperature of 80°C. The SnO<sub>2</sub> solution that has been evenly distributed and turns into a gel is then cooled in the air until the temperature is the same as the room temperature, which is 27°C. The plastic optical fiber's core was put into the SnO<sub>2</sub> gel, and after drying for two minutes under a heater set to 30°C, it was removed.

### 3.3 Experimental Setup

An OTDR (AQ7275, Yokogawa Inc.) was employed as this study's light source and light meter. OTDR is typically used to gauge signal or information loss during fiber optic light transmission. An OTDR can detect and show optical light pulses caused by Fresnel reflection or light backscattering at the optical fiber's end or endpoint. The benefit of OTDR is that it can measure various optical signal waveforms in real time over vast distances.

A plastic fiber optic test instrument for use as a gasoline and diesel vapor sensor is shown in Figure 8. A laptop serves as the main component of the data acquisition device. The OTDR device collects the information, transforming the light signal into voltage-based data (volts). There are air inlets and air outlets in the light-tight enclosure. The test case can benefit from introducing dry and wet air using air ducts. A heater automatically controlled by the appropriate test temperature is also included in the container. A thermocouple was used to gauge the test container's comparative temperature (971 temperature and humidity meter, fluke). A reference holder is located at the optical fiber's termination. The reference container can compare the test container's state to a baseline reference or typical condition. In other words, the reference value and the sensor reading value from the test case will be compared. When dealing with vapors, the comparison value changes into the change value.

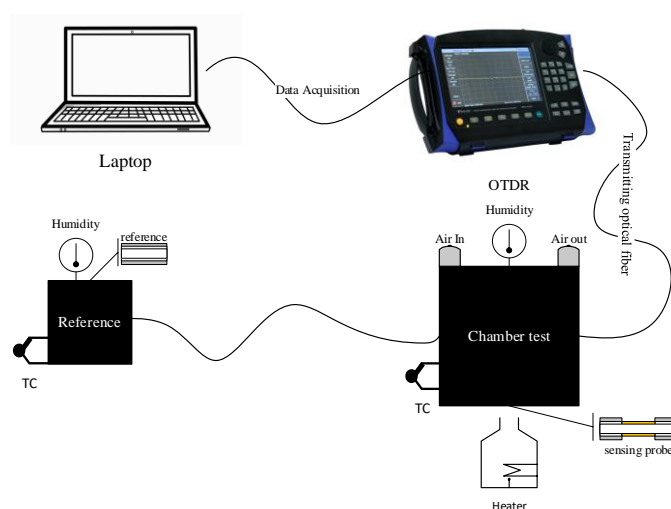


**Fig. 8.** Experimental device for detecting gasoline and diesel vapor.

## 4 Results and Discussion

When a plastic fiber optic sensor interacts with gasoline vapor or diesel vapor, the intensity of light propagating in the optical fiber will change. The strength of the optical fiber's light intensity (optical power) originates from the OTDR in the voltage change value. Furthermore, the value of the change in voltage is calculated from the difference between the sensor response voltage and the reference. The change value obtained when the fiber optic sensor interacts with gasoline or diesel vapor is compared with a reference. Fiber optic sensors are tested by varying the test case's temperature from 27 °C to 45 °C.

Plastic fiber optic sensors are tested by flowing dry air into the test container. Draining dry air is the first step in plastic fiber optic sensor testing. This stage is also carried out before testing the next sample vapors with a different vapor concentration. This initial stage aims to neutralize or clean the test container before adding gas or diesel vapor as a test sample. Dry air is circulated for 30 seconds. While testing gasoline and diesel vapor, the temperature level is set automatically from 27 °C to 45 °C.

Based on Table 1, each vapor concentration has a different coefficient of determination ( $R^2$ ). At the level of gasoline vapor concentration of 10 ppm, based on the test results obtained, a voltage value of -0.0012 volts for every one degree celsius increase in temperature, so the  $R^2$  obtained is 0.9747. At the gasoline vapor concentration level of 20 ppm, the voltage value for every 1 °C temperature increase is 0.0336 volts, so for each temperature variation,  $R^2$  is 0.9502. Testing at the level of gasoline vapor concentration of 30 ppm, the voltage value for each temperature increase of 1 °C is 0.0428 volts, and the  $R^2$  value for temperature variations is 0.7917. Testing at the level of gasoline vapor concentration of 40 ppm, the resulting voltage value for each temperature increase of 1 °C celsius is 0.0693 volts, and the  $R^2$  value for temperature variations is 0.7607. Testing at the gasoline vapor concentration level of 50 ppm, the voltage value for each temperature increase of 1°C celsius is 0.0821 volts, and the  $R^2$  value for different temperature variations is 0.7039.

**Table 1.** Light intensity (gasoline vapor)

Temp. (°C)	Optical Power (Volt)				
	10 ppm	20 ppm	30 ppm	40 ppm	50 ppm
27	2.951	3.079	3.361	3.490	3.587
29	2.949	3.141	3.538	3.842	4.089
31	2.947	3.110	3.456	3.669	3.851
33	2.946	3.183	3.623	3.970	4.225
35	2.944	3.228	3.706	4.075	4.359
37	2.943	3.258	3.729	4.110	4.421
39	2.942	3.330	3.761	4.173	4.430
41	2.941	3.310	3.755	4.164	4.430
43	2.941	3.352	3.761	4.172	4.430
45	2.939	3.366	3.758	4.158	4.430
Y	-0.0012x + 2.9511	0.0336x + 3.051	0.0428x + 3.4094	0.0693x + 3.601	0.0821x + 3.7737
$R^2$	0.9747	0.9502	0.7917	0.7607	0.7039

Figure 9 shows the relationship between gasoline vapor concentration and temperature. The plastic fiber optic sensor with the most accurate linear regression is tested at a gasoline vapor concentration of 10 ppm,  $R^2 = 0.9747$ . In addition, optical fiber has the greatest sensitivity seen from the transfer function, which is 0.0821 volts / °C.

Based on the data in Table 2, each vapor concentration has a different coefficient of determination ( $R^2$ ). At a concentration level of 10 ppm, diesel vapors, based on the test results, obtained a voltage value of -0.0308 volts for every one °C increase in temperature, so the  $R^2$  obtained is 0.9276. At 20 ppm diesel vapor concentration, the voltage value for every 1 °C temperature increase is -0.0224 volts, so for each temperature variation,  $R^2$  is 0.8778. Testing at the level of diesel vapor concentration of 30 ppm, the voltage value for each temperature increase per 1 °C is -0.02238 volts, and the  $R^2$  value for temperature variations is 0.9498. Testing at the level of diesel vapor concentration of 40 ppm, the voltage value for each temperature increase per 1 °C is -0.0289 volts, and the  $R^2$  value for temperature variations is 0.9538. Testing at the level of diesel vapor concentration of 50 ppm, the voltage value for each temperature increase per 1 °C is -0.0262 volts, and the  $R^2$  value for different temperature variations is 0.9593.

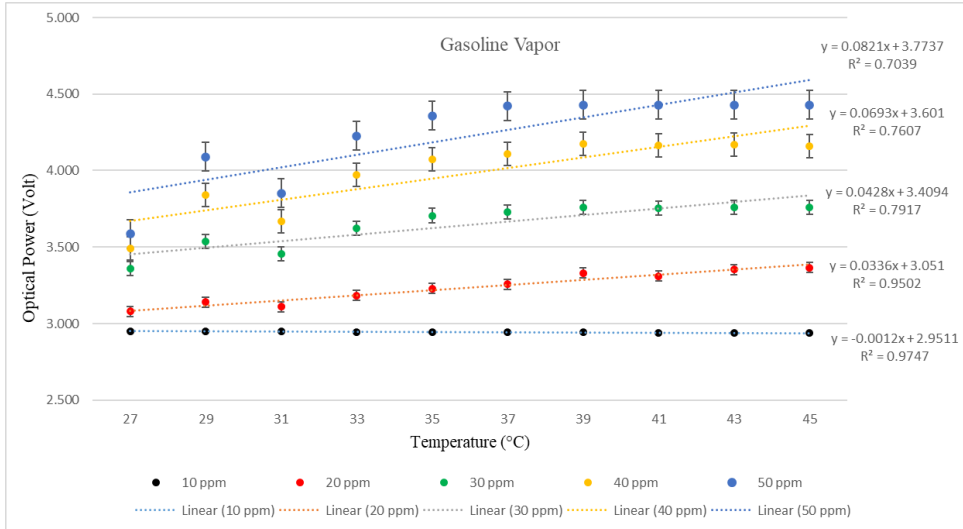


**Fig. 9.** The relationship between gasoline vapor concentration and temperature.

**Table 2.** Light intensity (diesel vapor)

Temp. (°C)	Optical Power (Volt)				
	10 ppm	20 ppm	30 ppm	40 ppm	50 ppm
27	2.652	2.835	3.042	3.192	3.306
29	2.551	2.787	2.987	3.113	3.234
31	2.517	2.770	2.967	3.065	3.198
33	2.492	2.761	2.946	3.048	3.183
35	2.479	2.755	2.905	3.037	3.173
37	2.469	2.750	2.869	3.011	3.142
39	2.458	2.732	2.856	2.967	3.098
41	2.404	2.694	2.850	2.940	3.084
43	2.342	2.652	2.844	2.929	3.074
45	2.325	2.582	2.816	2.904	3.044
Y	-0.0308x + 2.6384	-0.0224x + 2.855	-0.0238x + 3.0394	-0.0289x + 3.1795	-0.0262x + 3.298
R <sup>2</sup>	0.9276	0.8778	0.9498	0.9538	0.9593

Figure 10 illustrates the relationship between the concentration of diesel vapor with temperature. Based on the measurement of the most accurate linear regression obtained,  $y = -0.0262x + 3.298$ . The number  $-0.0262$  is the sensor's sensitivity, and  $3.298$  is the offset from the OTDR reading. The coefficient of determination ( $R^2$ ) obtained is  $0.9593$ , meaning it has fairly good linearity.

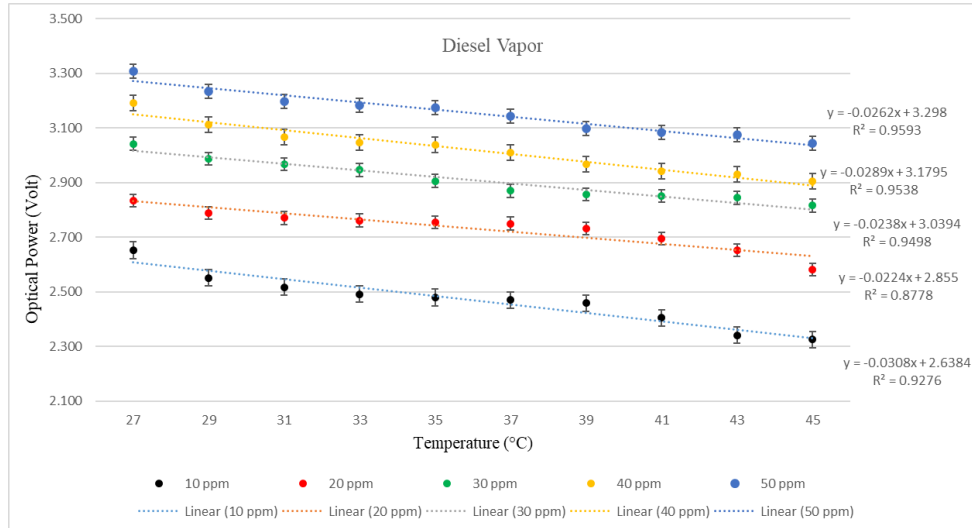


**Fig. 10.** The relationship between the concentration of diesel vapor with temperature.

Based on Figure 9, the graph shows that the higher the gasoline vapor concentration, the lower the light intensity received by the OTDR. The low light intensity caused by the increase in vapor concentration makes the refractive index of SnO<sub>2</sub> decrease due to swelling when absorbing gasoline vapor or diesel vapor. Suppose the refractive index of the cladding decreases. In that case, the depth of penetration of the evanescent wave will be greater so that more light enters the cladding and the intensity of light that propagates is smaller. What happens in Figure 10 is exactly the opposite of Figure 9, where the higher the concentration of diesel vapor, the higher the intensity of light received by the OTDR. These results indicate that the higher the light intensity received by the OTDR, the higher the voltage generated.

## 5 Conclusion

Based on the results of the research that has been carried out, it can be concluded that plastic optical fiber with SnO<sub>2</sub> cladding has been able to be used as a sensor for gasoline vapor and diesel vapors. SnO<sub>2</sub> coating as a replacement cladding using a 3 cm long dip-coating method at the center of the plastic optical fiber. The optical fiber sensor that has been made can respond to gasoline vapor concentrations, with the most optimal sensor sensitivity value being 0.0821 volts/°C at 50 ppm. In comparison, the response to diesel vapor has a sensitivity value of -0.0262 volts/°C at a concentration of 50 ppm.

There is a difference in the response of the fiber optic sensor when interacting with gasoline and diesel vapor. The higher the concentration of gasoline vapors, the less light the OTDR receives while interacting with them. The evanescent waves that travel farther into the sheathing produce reduced light intensity. Inversely related to the amount of diesel vapor that the sensor encounters. The higher the concentration of diesel vapor given, the more light intensity received by the OTDR. The SnO<sub>2</sub> layer's increased refractive index, which results from the fact that it does not absorb solar vapor, causes a rise in light intensity. Therefore, if the refractive index of the SnO<sub>2</sub> cladding increases, the depth of penetration of the evanescent

wave will be smaller so that less light enters the cladding and the intensity of light that propagates is smaller.

**Acknowledgment.** Through the Medan State University Research and Community Service Institute, the DIPA Fund of Medan State University funded this study in 2022.

## References

- [1] P. H. Suharti, W. Budhi, and Y. Bindar, "Kajian Pemanfaatan Reverse Flow Reactor untuk Oksidasi Katalik Uap Bensin," *Jurnal Teknik Kimia Indonesia*, vol. 10, no. 1, pp. 26–36, 2011, [Online]. Available: [www.bphmigas.go.id](http://www.bphmigas.go.id).
- [2] D. Paul, S. Dutta, and R. Biswas, "LSPR enhanced gasoline sensing with a U-bent optical fiber," *Journal of Physics D: Applied Physics*, vol. 49, no. 30, 2016, doi: 10.1088/0022-3727/49/30/305104.
- [3] A. Zanelli, S. Bassini, M. Giorgetti, Y. Li, and M. J. Yang, "Chemiresistors for ethanol detection in hydrocarbons," *Sensors and Actuators, B: Chemical*, vol. 148, no. 1, pp. 147–152, 2010, doi: 10.1016/j.snb.2010.04.037.
- [4] A. V. Kalach and V. F. Selemenev, "A piezoresonance sensor system for rapid evaluation of the quality of gasolines," *Chemistry and Technology of Fuels and Oils*, vol. 43, no. 1, pp. 60–63, 2007, doi: 10.1007/s10553-007-0012-z.
- [5] N. K. L. Wiziack *et al.*, "A sensor array based on mass and capacitance transducers for the detection of adulterated gasolines," *Sensors and Actuators, B: Chemical*, vol. 140, no. 2, pp. 508–513, 2009, doi: 10.1016/j.snb.2009.05.033.
- [6] B. D. Waluyo, R. D. Sari, and S. Januariyansah, "Testing and development of plastic optical fiber as humidity and temperature sensor," *Journal of Physics: Conference Series*, vol. 2193, no. 1, 2022, doi: 10.1088/1742-6596/2193/1/012071.
- [7] S. Aristilde, C. M. B. Cordeiro, and J. H. Osório, "Gasoline quality sensor based on tilted fiber bragg gratings," *Photonics*, vol. 6, no. 2, 2019, doi: 10.3390/photonics6020051.
- [8] D. Pawar, R. Kitture, and S. N. Kale, "ZnO coated Fabry-Perot interferometric optical fiber for detection of gasoline blend vapors: Refractive index and fringe visibility manipulation studies," *Optics and Laser Technology*, vol. 89, no. September 2016, pp. 46–53, 2017, doi: 10.1016/j.optlastec.2016.09.038.
- [9] B. R. Heidemann, G. R. C. Possetti, L. C. Côcco, C. I. Yamamoto, M. Muller, and J. L. Fabris, "Assessment of biodiesel-diesel blends with an optical fiber grating sensor," *SBMO/IEEE MTT-S International Microwave and Optoelectronics Conference Proceedings*, pp. 857–861, 2011, doi: 10.1109/IMOC.2011.6169226.
- [10] S. Agarwal, Y. K. Prajapati, and V. Mishra, "Thinned fibre Bragg grating as a fuel adulteration sensor: Simulation and experimental study," *Opto-Electronics Review*, vol. 23, no. 4, pp. 231–238, 2015, doi: 10.1515/oere-2015-0037.
- [11] G. R. C. Possetti, R. C. Kamikawachi, M. Muller, and J. L. Fabris, "Sensing ethanol-blended gasoline with long-period fiber grating: A metrological perspective," *Journal of Microwaves, Optoelectronics and Electromagnetic Applications*, vol. 12, no. SPL ISSU, pp. 9–17, 2013.
- [12] R. Falate, M. Müller, J. L. Fabris, and H. J. Kalinowski, "Long Period Gratings in Standard Telecommunication Optical Fibers for Fuel Quality Control," *Annals of Optics*, vol. 5, 2003.
- [13] A. J. R. Rodríguez, O. Baldovino-Pantaleón, R. F. D. Cruz, C. R. Zamarreño, I. R. Matías, and D.

- A. May-Arrijoja, "Gasohol quality control for real time applications by means of a multimode interference fiber sensor," *Sensors (Switzerland)*, vol. 14, no. 9, pp. 17817–17828, 2014, doi: 10.3390/s140917817.
- [14] S. Yin, P. B. Ruffin, and F. T. S. Yu, *Fiber Optic sensors*. CRC Press, 2008.
- [15] M. Sheeba, M. Rajesh, C. P. G. Vallabhan, V. P. N. Nampoori, and P. Radhakrishnan, "Fibre optic sensor for the detection of adulterant traces in coconut oil," *Measurement Science and Technology*, vol. 16, no. 11, pp. 2247–2250, 2005, doi: 10.1088/0957-0233/16/11/016.
- [16] E. Udd and W. B. Spillman, *Fiber Optic Sensors: An Introduction for Engineers and Scientists: Second Edition*. 2011.
- [17] Z. M. Tian *et al.*, "Structure and magnetic properties in Mn doped SnO<sub>2</sub> nanoparticles synthesized by chemical co-precipitation method," *Journal of Alloys and Compounds*, vol. 466, no. 1–2, pp. 26–30, 2008, doi: 10.1016/j.jallcom.2007.11.054.
- [18] A. Khorsand Zak, W. H. Abd. Majid, M. E. Abrishami, and R. Yousefi, "X-ray analysis of ZnO nanoparticles by Williamson-Hall and size-strain plot methods," *Solid State Sciences*, vol. 13, no. 1, pp. 251–256, 2011, doi: 10.1016/j.solidstatesciences.2010.11.024.